Electronic Supplementary Material (ESI) for Soft Matter.

Online supplementary information

Governing Equations

For the viscous flow, we assume that the liquid thickness is small compared to the film length ($H_0 \ll L$), and by using the lubrication approximation we obtain:

$$\frac{\partial p}{\partial x} = \eta \frac{\partial^2 v_x}{\partial z^2} \tag{S1}$$

where p is the pressure in the liquid, v_x is the flow velocity in the x-direction, and η is the liquid viscosity; the effect of gravity as a body force is ignored. The viscous shear stress in the liquid is:

$$\tau_{zx} = \eta \frac{\partial v_x}{\partial z} \tag{S2}$$

At the top surface of the liquid layer ($z = H$) a shear stress is transferred to the elastic film:

$$T = \eta \frac{\partial v_x}{\partial z}\Big|_{z=H} \tag{S3}$$

At the bottom of the liquid layer, we assume no-slip at the liquid/rubber interface and hence have the boundary condition:

$$v_x = \dot{\varepsilon} x \text{ at } z = 0 \tag{S4}$$

where $\dot{\varepsilon}$ is the strain rate of the rubber contraction, with $\dot{\varepsilon} < 0$ for compression. The velocity is set to be zero at $x = 0$ (center of the film) to eliminate rigid-body motion.

Assuming the pressure p is independent of z for the thin liquid layer and integrating Eq. (S1) with the boundary conditions in Eqs. (S3) and (S4), we obtain:

$$v_x(z) = \frac{1}{2\eta}\frac{\partial p}{\partial x} z(z - 2H) + \frac{T}{\eta} z + \dot{\varepsilon} x \tag{S5}$$

The flow rate in the *x*-direction is then:

$$Q_x = \int_0^H v_x dz = -\frac{H^3}{3\eta}\frac{\partial p}{\partial x} + \frac{T}{\eta}\frac{H^2}{2} + \dot{\varepsilon} x H \tag{S6}$$

Using the mass conservation equation for an incompressible fluid:

$$\frac{\partial H}{\partial t} + \frac{\partial Q_x}{\partial x} = 0 \tag{S7}$$

The liquid thickness H is related to the out-of-plane displacement *w* of the top surface:

$$H(x) = H_0 + w(x) \tag{S8}$$

Substituting Eqs. (S6) and (S8) into Eq. (S7), we obtain an evolution equation

$$\frac{\partial w}{\partial t} = -\frac{\partial Q_x}{\partial x} = \frac{\partial}{\partial x}\left(\frac{H^3}{3\eta}\frac{\partial p}{\partial x} - \frac{H^2}{2\eta}T - \dot{\varepsilon}xH\right) \tag{S9}$$

and the in-plane displacement u of the top surface is related to the flow velocity in Eq. (S5) as

$$\frac{\partial u}{\partial t} = v_x|_{z=H} = -\frac{H^2}{2\eta}\frac{\partial p}{\partial x} + \frac{H}{\eta}T + \dot{\varepsilon}x \tag{S10}$$

For the elastic film, the equations are similar to Huang and Suo [13], except that there is no prestrain, but instead there are terms corresponding to the applied strain rate. The in-plane normal stress in the film is:

$$\sigma = \frac{E}{1-\nu^2}\left[\frac{\partial u}{\partial x} + \frac{1}{2}\left(\frac{\partial w}{\partial x}\right)^2\right] \tag{S11}$$

where E and ν are Young's modulus and Poisson's ratio of the elastic film, respectively. Subject to the viscous shear stress T across the film/liquid interface, force balance within the film requires that:

$$T = h\frac{\partial \sigma}{\partial x} \tag{S12}$$

In addition, a force balance perpendicular to the plane of the film yields:

$$p = D\frac{\partial^4 w}{\partial x^4} - \sigma h\frac{\partial^2 w}{\partial x^2} - T\frac{\partial w}{\partial x} \tag{S13}$$

Here D is the flexural rigidity of the elastic film: $D = \dfrac{Eh^3}{12(1-\nu^2)}$.

The boundary conditions to be applied at the ends of the film with $x = \pm L$ are:

No normal stress $$\frac{\partial u}{\partial x} + \frac{1}{2}\left(\frac{\partial w}{\partial x}\right)^2 = 0 \tag{S14}$$

No bending moment $$\frac{\partial^2 w}{\partial x^2} = 0 \tag{S15}$$

No shear force $$\frac{\partial^3 w}{\partial x^3} = 0 \tag{S16}$$

No pressure $$D\frac{\partial^4 w}{\partial x^4} - T\frac{\partial w}{\partial x} = 0 \tag{S17}$$

These are the same equations as Liang et al, (Acta Mater. **50**, 2933, 2002). The above equations can be non-dimensionalized by the scaled parameters as described in the main text, yielding the dimensionless evolution equations and boundary conditions given in the main text (Eqs. 1-6).

Linear Perturbation Analysis

Using Eqs. 20 and 21 in the main text as perturbations, the displacements can be written as a sum of the base (shear lag) solution and the perturbation:

$$w_s = w_s^{sh} + w_s^p \tag{S18}$$

and

$$u_s = u_s^{sh} + u_s^p \tag{S19}$$

where we denote the shear lag solutions with the superscript "sh". Substituting these values for u_s and w_s in the governing equations, subtracting the base equations i.e. the shear lag solutions (see main text), and neglecting nonlinear terms of the perturbation, we obtain the linear evolution equations for the displacement perturbations. The evolution for w_s can be written as:

$$\begin{aligned}\Omega_s B_0 = \Bigg[& \frac{1}{3} H_{s0}^3 \frac{\partial^2 p_s^p}{\partial x_s^2} - H_{s0} w_s^{sh} \left(\frac{1}{12} k_s{}^6 B_0 \right) + H_{s0}^2 \frac{\partial w_s^{sh}}{\partial x_s} \left(\frac{1}{12} i k_s{}^5 B_0 \right) \\ & - H_{s0} B_0 \frac{\partial^3 u_s^{sh}}{\partial x_s^3} - H_{s0} (i k_s B_0) \frac{\partial^2 u_s^{sh}}{\partial x_s^2} - \left(\frac{H_{s0}^2}{2} + H_{s0} w_s^{sh} \right) (k_s{}^3 A_0) + \left(H_{s0} \frac{\partial w_s^{sh}}{\partial x_s} \right) (k_s{}^2 i A_0) \\ & - \beta x_s (i k_s B_0) - \beta B_0 \Bigg]\end{aligned} \tag{S20}$$

Similarly, the corresponding evolution of the in-plane displacement can be written as:

$$\Omega_s A_0 = \left[i \frac{(H_{s0})^2}{2} \frac{\partial p_s^p}{\partial x_s} - H_{s0} w_s^{sh} \frac{k_s{}^5 B_0}{12} - H_{s0} (k_s{}^2 A_0) - w_s^{sh} (k_s{}^2 A_0) - i B_0 T_s^{sh} \right] \tag{S21}$$

In deriving these equations, terms containing $d\Omega_s/dt$ have been neglected, which is equivalent to assuming that the time-scale over which perturbations grow is very different from the time-scale over which the shear lag solution evolves.

The first derivative of pressure is written as:

$$\begin{aligned}\frac{\partial p_s^p}{\partial x_s} = & \frac{1}{12} i k_s{}^5 B_0 + N_s^{sh} (i k_s{}^3 B_0) + (k_s A_0) \frac{\partial^3 w_s^{sh}}{\partial x_s^3} + 2 T_s^{sh} (k_s{}^2 B_0) \\ & + 2 (k_s{}^2 i A_0) \frac{\partial^2 w_s^{sh}}{\partial x_s^2} - \frac{\partial T_s^{sh}}{\partial x_s} (i k_s B_0) - (k_s{}^3 A_0) \frac{\partial w_s^{sh}}{\partial x_s}\end{aligned} \tag{S22}$$

and the second derivative as:

$$\begin{aligned}\frac{\partial^2 p_s}{\partial x_s^2} = & -\frac{1}{12} k_s{}^6 B_0 - N_s^{sh} (k_s{}^4 B_0) + (k_s A_0) \frac{\partial^4 w_s^{sh}}{\partial x_s^4} + 3 T_s^{sh} (i k_s{}^3 B_0) + 3 (i k_s{}^2 A_0) \frac{\partial^3 w_s^{sh}}{\partial x_s^3} \\ & + 3 \frac{\partial T_s^{sh}}{\partial x_s} (k_s{}^2 B_0) - 3 (k_s{}^3 A_0) \frac{\partial^2 w_s^{sh}}{\partial x_s^2} - \frac{\partial^2 T_s^{sh}}{\partial x_s^2} (i k_s B_0) - (k_s{}^4 i A_0) \frac{\partial w_s^{sh}}{\partial x_s}\end{aligned} \tag{S23}$$

Thus Eqs. (S41) and (S42) can be represented as an eigenvalue problem of the form:

$$\Omega_s \begin{bmatrix} B_0 \\ A_0 \end{bmatrix} = \begin{bmatrix} M_{11} & M_{12} \\ M_{21} & M_{22} \end{bmatrix} \begin{bmatrix} B_0 \\ A_0 \end{bmatrix} \tag{S24}$$

where M_{11}, M_{12}, M_{21}, M_{22} are complex numbers, and functions of t_s and k_s.

The eigenvalues of the M matrix are the instantaneous growth rate Ω_s. The shear lag solution can be regarded as being unstable if the real part of the eigenvalue is positive. The eigenvalues were computed for various values of k_s using MATLAB (Mathworks Inc.). Of the two eigenvalues obtained from the equation, the one with the greater real part is considered as the dominant growth rate.

Quantitative comparison of linear perturbation analysis vs experiments

Figs. 7 and 11 in the main text respectively showed the fastest growing wavenumber predicted by linear perturbation analysis, and the wavelength observed experimentally. Fig. S1 compares them directly in non-dimensional form. The symbols are measured wavenumber at one specific liquid thickness, $H_0 = 0.9\ mm$ ($H_{s0} = 36$): filled points are same data as in Fig. 11a, whereas open points are two more experimental runs at the same liquid layer thickness. The solid line is a fit to the k_{sm} predicted by the linear perturbation analysis, i.e. it is the same as the solid line in Fig. 7a in the main text. In the experimental range, the linear perturbation analysis typically predicts the wavenumber to be roughly twice of what is observed experimentally.

Section 3 in the main text discussed the analogy between the situation at hand (film being compressed at a specified rate) and the situation where a film with a compressive prestrain ε_0 rests on a viscous liquid. Fig. 6 in the main text showed that the dispersion relation is similar in these two situations if the prestrain is assigned the value of the instantaneous strain. Here we will test this analogy against experiments taking advantage of the fact that in all our experiments, buckles appear at long times (i.e. $t \gg \tau$), when the scaled compressive stress has a value of σ_s^{max}. For the experimental value of $H_{s0} = 36$, it is reasonable to take the limit of an infinitely thick liquid layer considered by Sridhar et al (Appl. Phys. Lett. **78**, 2482, 2001). In that limit, the fastest-growing wave number is predicted to be $\sqrt{4\varepsilon_0(1+\nu)}$. Pursuing this analogy, we replace ε_0 with $|\sigma_s^{max}|$, thus giving the prediction that $k_{sm} = \sqrt{4\left(\frac{|\beta|L_s^2}{2H_{s0}}\right)(1+\nu)}$. This prediction, also plotted in Fig. S1, is up to 50% higher than the experiments.

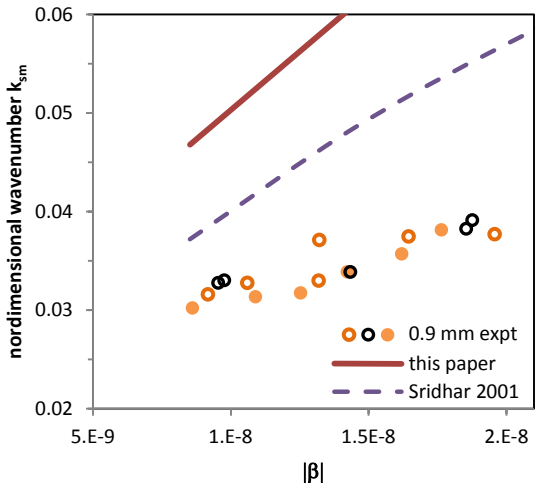

Fig. S1: Dimensionless wave number vs dimensionless compression rate. Solid symbols are the same as the 0.9 mm data in Fig. 11a in the main text. Open points are two more runs at the same liquid layer thickness. Solid line is a fit to the linear perturbation results, i.e. same as the solid line in Fig.7a in the main text. For explanation of dashed line, see above.

Numerical simulations

A numerical method based on a finite difference scheme was adopted, with center difference for space discretization and implicit backward difference for time integration. The method is similar to Liang et al. (Acta Mater. **50**, 2933, 2002), using fictitious nodes at each end to satisfy the boundary conditions. For each time step, the solution was obtained by iteration using the Newton-Raphson method.

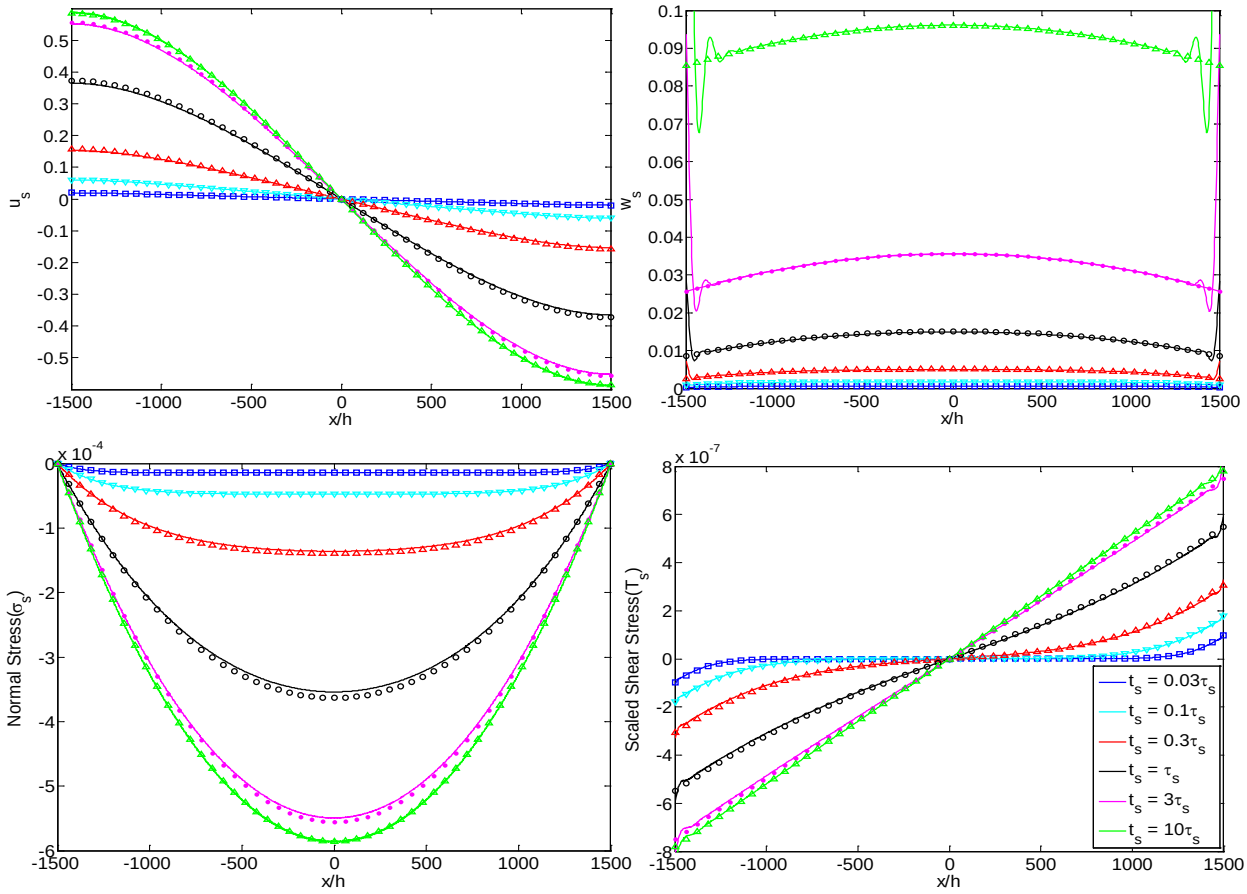

Fig. S2: Comparison of numerical simulation (solid lines) with the shear lag solution (symbols) at short times ($t_s \leq 10\tau_s$).

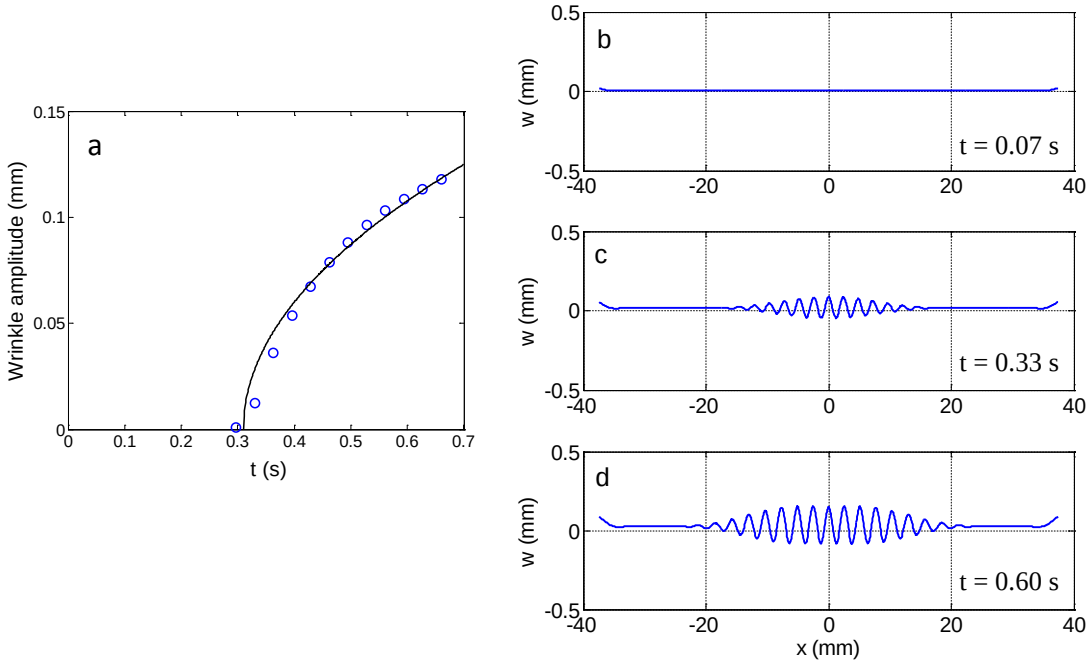

Fig. S3: Numerical simulation using the same parameters as the experiment of Fig. 8 in the main text ($2L$ = 75 mm; h = 25 μm; H_0 = 0.9 mm; $\dot{\varepsilon} = -0.088s^{-1}$). **a**. Evolution of wrinkle amplitude with time. The solid line indicates a simple power law: $A = k(t - t_c)^{0.5}$, with $t_c = 0.31s$. **b**-**d**. Simulated wrinkle profiles at various times, corresponding to Fig. 8b-d.

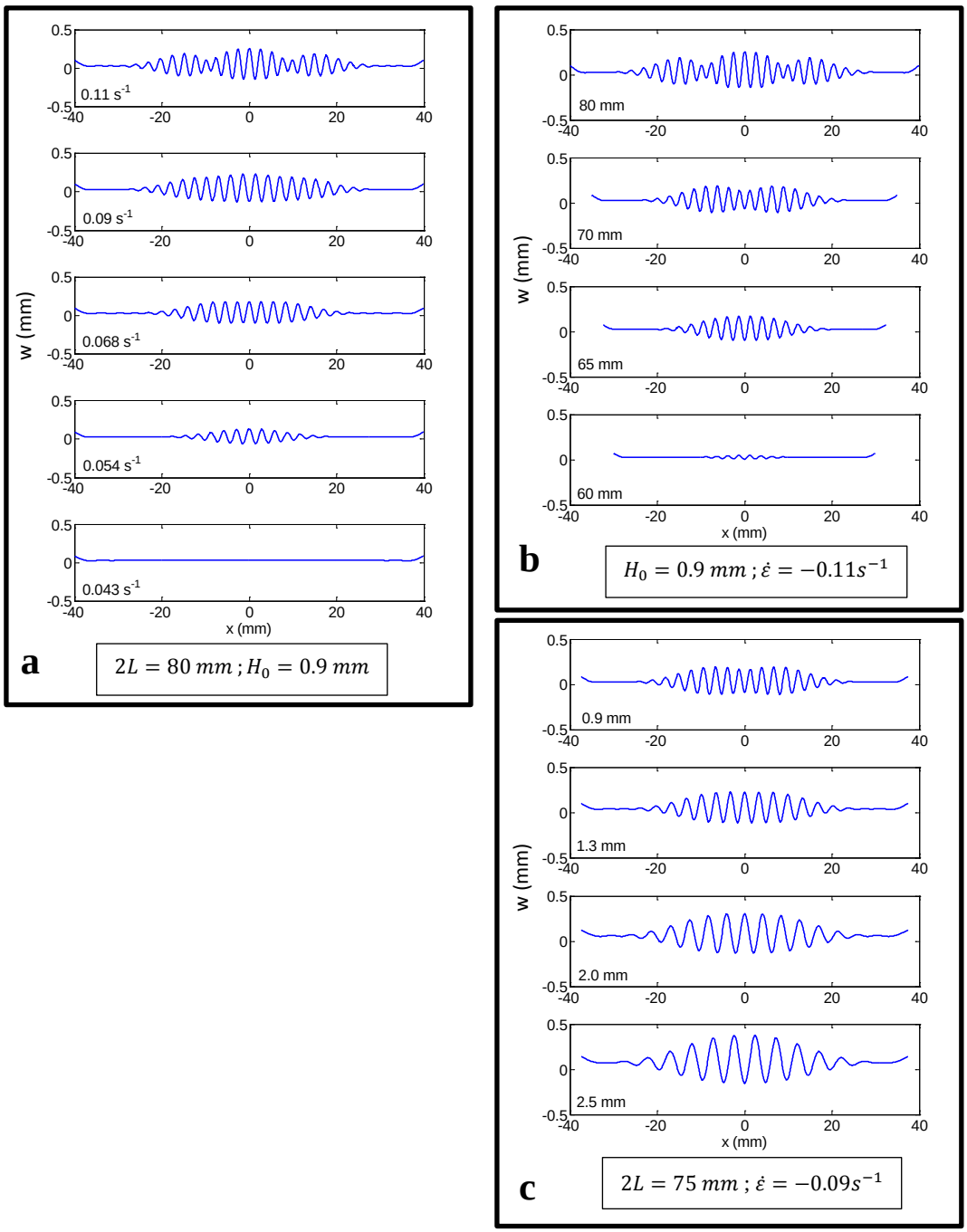

Fig. S4: Simulations approximately matching the conditions in the three panels in Fig. 9 in the main text, showing the effect of each of the three parameters on wrinkling. In all graphs, the y-axis is the dimensional value (in mm) of the out-of-plane displacement. Each graph corresponds to $\dot{\varepsilon}t = 0.06$.